



# The determination of the activities of different iron species in Fe-ZSM-5 for SCR of NO by NH<sub>3</sub>

Sandro Brandenberger<sup>a</sup>, Oliver Kröcher<sup>a,\*</sup>, Arno Tissler<sup>b</sup>, Roderik Althoff<sup>b</sup>

<sup>a</sup> Paul Scherrer Institute, 5232 Villigen PSI, Switzerland

<sup>b</sup> Süd-Chemie AG, Waldheimer Str. 15, 83052 Bruckmühl, Germany

## ARTICLE INFO

### Article history:

Received 27 October 2009

Received in revised form 14 January 2010

Accepted 18 January 2010

Available online 25 January 2010

### Keywords:

SCR

Selective catalytic reduction

Ammonia

NO<sub>x</sub> reduction efficiency

Fe-ZSM-5

Zeolite

Active sites

## ABSTRACT

The activities of different iron species in Fe-ZSM-5 for the selective catalytic reduction (SCR) of NO by NH<sub>3</sub> were determined in terms of their turnover frequencies (TOF values). The relative concentrations of different species were correlated with their measured NO<sub>x</sub> reduction efficiencies and NH<sub>3</sub> oxidation activities. Our results suggest that the SCR of NO by NH<sub>3</sub> is catalyzed by different active sites with different activation energies. At temperatures below 300 °C, the SCR activity was observed to be primarily caused by monomeric iron sites; however, at  $T > 300$  °C,  $T \geq 400$  °C and  $T \geq 500$  °C, the contribution of dimeric iron species, oligomeric species (e.g., trimeric and tetrameric iron species) and partially uncoordinated iron sites in the outmost layer of iron oxide particles, respectively, become important. The activation energies for monomeric and dimeric sites were evaluated to be about 36 kJ/mol and 77 kJ/mol, respectively. Due to their high activation energies, dimeric sites contributed more to the overall SCR activity at higher temperatures than did monomeric sites. The clustered sites not only contributed to the SCR activity but also caused nonselective oxidation of NH<sub>3</sub> at  $T \geq 350$  °C, whereas the dimeric species governed the NH<sub>3</sub> oxidation activity up to  $T = 500$  °C. The TOF values for dimeric species were estimated to be  $70 \pm 13$  s<sup>-1</sup> at 500 °C. Monomeric sites were found to be completely inactive for NH<sub>3</sub> oxidation up to 500 °C.

© 2010 Elsevier B.V. All rights reserved.

## 1. Introduction

Selective catalytic reduction (SCR) with ammonia-containing precursors, such as urea, is an efficient method to eliminate NO<sub>x</sub> emissions from the exhaust of diesel vehicles and stationary combustion processes [1–3]. Many metal-exchanged zeolites (ZSM-5, MOR, BEA and FER) have been shown to be active catalysts for the NH<sub>3</sub>-SCR of NO [4,5]. Among these options, Fe-ZSM-5 provides an optimal combination of catalytic activity and stability over a broad temperature range [6,7].

Despite the current large body of research focusing on the details of SCR chemistry in iron-exchanged zeolites, the identity and nuclearity of SCR active sites is still the subject of much discussion for these types of catalysts. Different types of active sites have been postulated, including small Fe<sub>x</sub>O<sub>y</sub>(OH)<sub>z</sub> clusters, such as Fe<sub>4</sub>O<sub>4</sub>; oxygen-bridged binuclear iron species, such as [HO–Fe–O–Fe–OH]<sup>2+</sup> [8–15]; monomeric Fe<sup>2+</sup> and Fe<sup>3+</sup> ions [10,11,16–19]; extra-framework Fe–O–Al [20]; and grafted Fe–O–Si [21] species. Krishna and Makkee [18] ruled out the extensive formation of Fe–O–Al species, even under extreme reaction

conditions (700 °C and a high concentration of gas-phase HCl). Furthermore, infrared spectroscopy has shown [22] that Fe–O–Si species do not form to a significant extent in Fe-ZSM-5. This observation can be explained on the basis of DFT calculations, which have demonstrated a low affinity of transition metals for the oxygen atom of SiO<sub>4</sub> [23]. Therefore, the issue of the active sites can be reduced to whether monomeric metal ions or clustered species catalyze the SCR reaction. Among the different types of iron species, several research groups have favored binuclear iron, while monomeric species have been proposed much less frequently. Grünert [11,16,19] has proposed that monomeric iron species and bridged iron species contribute to NH<sub>3</sub>-SCR for iron-zeolites. Additionally, Joyner and Stockenhuber [13] have suggested that both clustered and monomeric iron ions are active at 500 °C, but the latter displays a relatively low activity. An analysis of available SCR activity data show that, in all probability, both species are active for the NH<sub>3</sub>-SCR of NO with the monomeric species being the most active species at low temperatures [24].

The clear identification of the active sites is primarily impeded by the absence of a suitable method for characterizing the nuclearity of the iron centers. In Fe-ZSM-5, monomeric iron species, binuclear and oligomeric clusters and iron oxide particles exist simultaneously. Due to the coexistence of these complex iron structures, the quantitative analysis of the different iron species

\* Corresponding author. Tel.: +41 56 310 20 66; fax: +41 56 310 23 23.  
E-mail address: [oliver.kroecher@psi.ch](mailto:oliver.kroecher@psi.ch) (O. Kröcher).

poses a serious problem. Many techniques have been applied toward the characterization of Fe-ZSM-5 (e.g., UV–vis, EPR, EXAFS, XPS, H-TPR, FTIR, Mössbauer and XRD); however, none have been able to confidently distinguish between the monomeric iron species and the iron oxide clusters of different nuclearity when they coexist in the same sample [25–27].

Recently, we suggested a method that allows for the estimation of the concentration of monomeric and clustered iron species by calculating the statistical distribution of monomeric and neighboring iron sites as a function of the iron loading (Fe/Al) for a given zeolite [25]. This method is based on the structural data for the position of all of the tetrahedral sites and it assumes an overall statistical distribution of aluminum and iron atoms.

The goal of the present study is to correlate the calculated quantity of monomeric and clustered iron sites with the measured  $\text{NO}_x$  reduction efficiencies. This correlation enables the evaluation of the relevance of the different iron species within the SCR reaction.

## 2. Experimental

### 2.1. Sample preparation

Different Fe-ZSM-5 ( $x$ ) ( $x = \text{Fe/Al}$ ) catalysts were prepared with a template-free synthesized  $\text{NH}_4$ -ZSM-5 zeolite (Süd-Chemie AG, Si/Al = 14) by liquid ion exchange and chemical vapor deposition (CVD) and coated on cordierite monoliths (400 cpsi) according to the methods described in detail in Ref [28]. For reliable results, it is essential that the degree of iron clustering and, therefore, the relative contents of the different iron species primarily depend on the iron content and not on the exchange method. To this end, we used a liquid ion exchange method that excelled in the formation of particularly homogeneous iron distributions [25]. The primary features of this method were the application of high temperature (80 °C), long exchange time (24 h), relative highly concentrated exchange solution (3–8 g  $\text{FeCl}_2/\text{l}$ ) and the addition of ammonium chloride to the reaction mixture to control the degree of exchange. Moreover, because it was proposed in the literature that the presence of templates might influence the Al substitution pattern [29–32], all Fe-ZSM-5 samples were prepared with a template-free synthesized zeolite.

H-ZSM-5 containing various sizes of  $\text{Fe}_2\text{O}_3$  particles was prepared according to the procedures outlined here. H-ZSM-5 consisting of 45–63  $\mu\text{m}$ -sized  $\text{Fe}_2\text{O}_3$  particles was prepared by physically mixing the aforementioned zeolite with iron oxide of the appropriate sieve fraction. H-ZSM-5 with 22 nm  $\text{Fe}_2\text{O}_3$  particles was prepared by precipitation of  $\text{FeCl}_3$  solution, in which the zeolite powder was suspended, at about a pH of 9. H-ZSM-5 with 9 nm-sized  $\text{Fe}_2\text{O}_3$  particles was prepared using previously published methods [33,34]. This process required coprecipitation from a ferrous/ferric mixed salt-solution in an alkaline medium in the presence of sodium oleate and subsequent calcination in air at 550 °C.

### 2.2. Catalyst characterization and activity measurements

Inductively coupled plasma-atomic emission spectroscopy (ICP-AES) was employed to quantify the elemental composition of the samples.

Activity measurements for the SCR reaction and  $\text{NH}_3$  oxidation were obtained in a heated quartz reactor. The concentrations of NO,  $\text{NO}_2$  and  $\text{NH}_3$  were analyzed by FT-IR spectroscopy using a Nicolet Magna IR 560 spectrometer equipped with a liquid nitrogen cooled MCT detector. The gas cell was heated to a temperature between 175 °C and 180 °C, thus preventing water condensation. More details on the set-up of the test apparatus have

been described elsewhere [35]. The gas compounds NO,  $\text{NO}_2$  and  $\text{NH}_3$  were quantified with a multi-component method developed in-house, which used OMNIC<sup>®</sup> Quantpad software. This technique is based on the classical least-squares (CLS) quantitative analysis algorithm and allows for the correction of nonlinear absorbance versus concentration. By implementing our accurate gas analysis method, in combination with coated monoliths that can be prepared with high precision and reproducibility [36], we were able to achieve a measurement uncertainty (expressed as standard deviation) of only 5% in the conversion range of 10–70%. This value was determined with three independently coated monoliths, which were measured on different days. The detection limits were found to be 1 ppm for NO and  $\text{NO}_2$  and 0.2 ppm for  $\text{NH}_3$ . The composition of diesel exhaust gas was approximated by a model feed gas containing 10%  $\text{O}_2$ , 5%  $\text{H}_2\text{O}$ , 1000 ppm of NO and  $\text{NH}_3$  and  $\text{N}_2$  as the balance. The NO conversion was investigated over H-ZSM-5 and Fe-ZSM-5 at GHSV = 52,000  $\text{h}^{-1}$  and 200,000  $\text{h}^{-1}$  with a feed gas consisting of 10%  $\text{O}_2$ , 5%  $\text{H}_2\text{O}$ , 1000 ppm  $\text{NH}_3$ , 1000 ppm NO and  $\text{N}_2$  as the balance.  $\text{NH}_3$  oxidation was investigated over H-ZSM-5 and Fe-ZSM-5 at GHSV = 52,000  $\text{h}^{-1}$  with a feed gas consisting of 10%  $\text{O}_2$ , 5%  $\text{H}_2\text{O}$ , 1000 ppm  $\text{NH}_3$  and  $\text{N}_2$  as the balance.

The kinetic constants of two catalysts were determined using the same set-up used for the activity measurements. For measuring the reaction order with respect to a certain reactant, the concentrations of the other gas components were kept constant while the concentration of the reactant was varied. The space velocity was 52,000  $\text{h}^{-1}$  for measurements between 210 °C and 325 °C and 200,000  $\text{h}^{-1}$  for measurements at 350 °C and 400 °C. Please note that the analysis at 200 °C was hampered due to a long-term drift, most likely caused by the slow formation of  $\text{NH}_4\text{NO}_3$  during the analysis.

## 3. Results

### 3.1. Active sites and catalytic activity

Table 1 summarizes the relative contents of the monomeric, dimeric, clustered and oligomeric species in the prepared zeolite samples, as determined by calculations in our previous study [25]. The results of an independent check of the calculations by UV–vis spectroscopy are also provided in Table 1. Please note that by UV–vis the concentrations of clustered species were not accessible [25]. Consequently, the calculated concentrations were employed for the evaluation of the following experiments.

Fig. 1 highlights the  $\text{NO}_x$  reduction efficiencies of Fe-ZSM-5 catalysts with different exchange degrees (Fe/Al) at GHSV = 52,000  $\text{h}^{-1}$  (a) and 200,000  $\text{h}^{-1}$  (b). Note that, for the samples with Fe/Al = 0.45 and 0.16, no SCR measurements at GHSV = 200,000  $\text{h}^{-1}$  were performed. All of these catalysts were prepared by liquid ion exchange, except for the sample with Fe/Al = 0.74, which was prepared by CVD. Remarkably, in Fig. 1a, at temperatures below 350 °C,  $\text{NO}_x$  conversion generally increased with increasing iron content, whereas at temperatures above 500 °C, the conversion level decreased with increasing iron content. Furthermore, at temperatures greater than 500 °C, there was a decrease in the  $\text{NO}_x$  conversion as a function of increasing temperature. Note that, for the very lowly and very highly exchanged zeolites with Fe = 0.02, 0.04 and 0.74, some of these trends were not observed; the reasons for this pattern will be discussed later.

The NO conversions of the Fe-ZSM-5 samples in Fig. 1 were corrected with the SCR activity of H-ZSM-5 and, on this basis, apparent turnover frequencies (TOF = number of converted NO molecules per second per iron center) were calculated as functions of the Fe/Al ratio (Fig. 2) related to the total iron content. In general, the apparent TOF values were calculated from data where the NO conversion was  $\leq 37\%$ . Only at  $T = 400$  °C for samples with Fe/

**Table 1**

Relative concentration of monomeric, dimeric, clustered and oligomeric species in the Fe-ZSM-5 samples, calculated according to Ref. [25].

Fe/Al	Fe [wt.%]	Monomeric species [%]	Clustered species (dimeric and oligomeric species) [%]	Dimeric species [%]	Oligomeric species [%]
		$\begin{array}{c} \text{OH} \\   \\ \text{Fe}^{3+} \\   \\ \text{---} \end{array}$		$\begin{array}{c} \text{HO} \quad \text{O} \quad \text{OH} \\   \quad / \quad \backslash \quad   \\ \text{Fe} \quad \quad \text{Fe} \end{array}$	$\text{Fe}_x\text{O}_y(\text{OH})_z \quad x \geq 3$
		a			b
0.02	0.14	95	100	5	1
0.04	0.27	90	92	10	2
0.08	0.56	79	78	21	6
0.15	1	68	74	32	14
0.16	1.1	66	78	34	16
0.3	2	46	44	54	38
0.39	2.6	37	30	63	50
0.45	3	31	–	69	58
0.74	5	15	11	85	81

<sup>a</sup> Measured by UV–vis spectroscopy. Sub-bands at  $\lambda \leq 290$  nm.<sup>b</sup> Difference between the concentration of clustered and dimeric species.

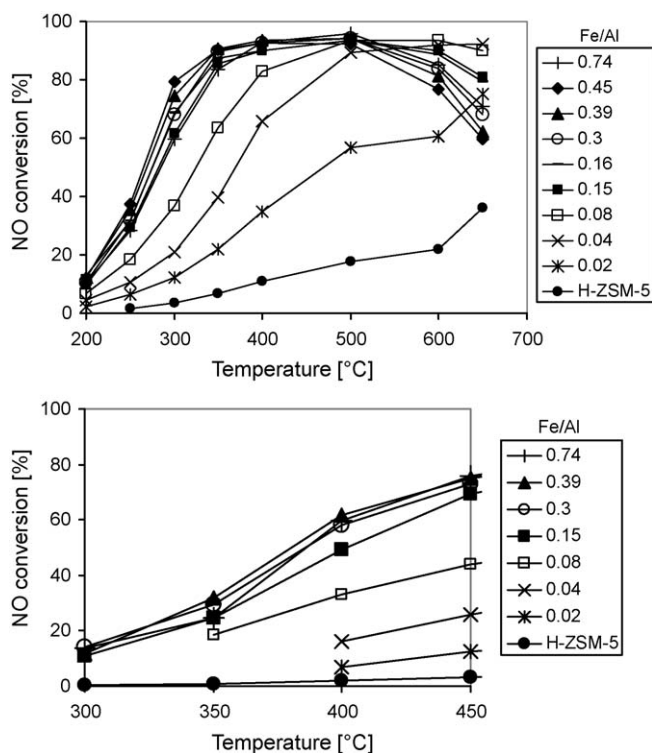
Al = 0.15, 0.39 and 0.74 were values of about 60% used. The results in Fig. 2 suggest that the activity calculated per iron center increased when the degree of iron exchange between 200 °C and 300 °C was reduced. In contrast, the calculated apparent TOF values indicate a higher activity per iron center above 300 °C for the zeolites with Fe/Al = 0.08 and 0.15, as compared to the zeolites with a very low exchange (Fe/Al = 0.02 and 0.04). Remarkably, for the higher exchange degrees (Fe/Al = 0.3, 0.39, and 0.74), we once again observed decreasing apparent TOF values.

Fig. 3 demonstrates that, beyond a temperature threshold of  $T \geq 500$  °C, the iron oxide particles located at the outside of the zeolite pores became species with significant SCR activities. Particles with an average size of 9 nm showed significantly greater NO conversion than the larger ones, which was attributed to an

increased number of unsaturated iron atoms on the surfaces of smaller particles [37].

The selective catalytic oxidation of  $\text{NH}_3$  to nitrogen is the most important side-reaction of the SCR reaction. This reaction was investigated in a separate experiment by dosing ammonia, oxygen and water without NO. The samples containing almost exclusively monomeric iron species (Fe/Al = 0.02 and 0.04) displayed no  $\text{NH}_3$  oxidation activity up to 500 °C, whereas high  $\text{NH}_3$  oxidation activities were found for samples with higher iron contents and corresponding higher degrees of clustering (Fig. 4). At higher temperatures, the high oxidation potential of clustered iron species were responsible for the oxidation of the reducing agent,  $\text{NH}_3$ , thereby limiting NO conversion in the SCR reaction. This observation was found to be consistent with current literature (e.g., [19]). Remarkably, at 500 °C,  $\text{NH}_3$  conversion reached a maximum of 88% for a medium exchange degree of Fe/Al = 0.45, whereas the conversion decreased for both lower and higher iron concentrations.

Fig. 5 illustrates that  $\text{Fe}_2\text{O}_3$  nanoclusters and particles also contributed to  $\text{NH}_3$  oxidation at  $T > 500$  °C. Small nanoclusters, with an average size of 9 nm, showed slightly higher activities than those with an average size of 22 nm. These particles were also considerably more active than the large particles with diameters between 45  $\mu\text{m}$  and 63  $\mu\text{m}$ . At temperatures greater than 500 °C, the oxidation of  $\text{NH}_3$  produced nitrogen and NO [24], as shown in Fig. 6, which further reduced the observed  $\text{NO}_x$  conversion in the SCR reaction. It appeared that the NO formation was more pronounced for zeolites with higher exchange degrees (e.g., Fe/Al = 0.45), less pronounced for zeolites with very high loading (Fe/Al = 0.74) or with middle loading (e.g., Fe/Al = 0.15) and even absent for zeolites with low loading (Fe/Al = 0.04). In Fig. 6, the feed



**Fig. 1.** NO reduction as a function of temperature over Fe-ZSM-5 catalysts with various exchange degrees. Reaction conditions: 1000 ppm NO, 1000 ppm  $\text{NH}_3$ , 10%  $\text{O}_2$ , 5%  $\text{H}_2\text{O}$  and  $\text{N}_2$  balance. (a) GHSV = 52,000  $\text{h}^{-1}$  and (b) GHSV = 200,000  $\text{h}^{-1}$ .

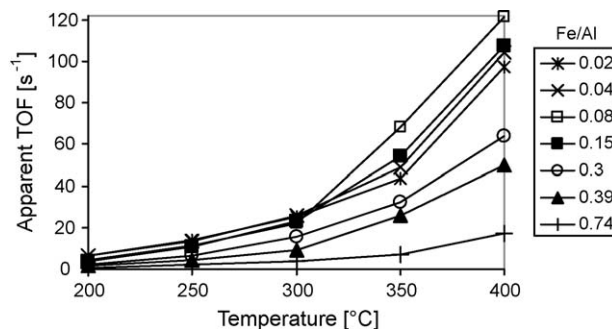


**Fig. 2.** Calculated number of converted NO molecules per second per iron center (apparent TOF) as a function of the Fe/Al ratio of the total iron content.

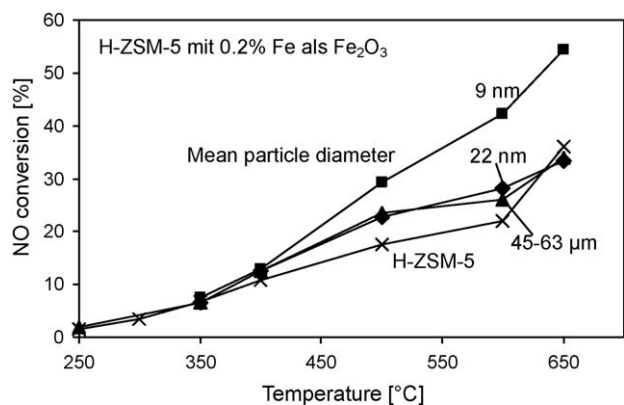


**Fig. 3.** NO reduction as a function of temperature over H-ZSM-5 samples coated with equal amounts of  $\text{Fe}_2\text{O}_3$  (0.2% Fe), across various particle sizes. Reaction conditions: 1000 ppm NO, 1000 ppm  $\text{NH}_3$ , 10%  $\text{O}_2$ , 5%  $\text{H}_2\text{O}$  and  $\text{N}_2$  balance. GHSV =  $52,000 \text{ h}^{-1}$ .

contained 1000 ppm  $\text{NH}_3$ , which meant that, over the zeolite with  $\text{Fe}/\text{Al} = 0.45$ , 10% of the  $\text{NH}_3$  was oxidized to NO at 650 °C. In regard to the particles, it was interesting to note that the formation of NO was more pronounced over 22 nm nanoclusters than over either smaller nanoclusters (9 nm) or larger particles (45–63  $\mu\text{m}$ ).

#### 4. Discussion

##### 4.1. Relation between structure of the active site and SCR activity

The experimental results in Fig. 2 reveal that, at  $T \leq 300$  °C, the iron sites in Fe-ZSM-5 generally show a higher apparent TOF value in samples with a low exchange degree, in which the iron is more “diluted” than in the highly exchanged samples. It is therefore reasonable to assume that the active sites at  $T \leq 300$  °C contain only a small number of iron atoms, or more likely, single atoms. This argumentation could be confirmed on a quantitative basis by calculating the fractions of different iron species. In Fig. 7, the apparent TOFs from Fig. 2 were recalculated with respect to monomeric iron species only. These TOF values fall together between 200 °C and 300 °C, suggesting that in this temperature regime, the active species in these catalysts are monomeric iron ions. This result is in line with the findings of Iwasaki et al. [38] who estimated the number of active sites by  $\text{NO}_2$ -TPD between 200 °C and 250 °C and concluded that all iron sites active in this temperature region (which are the monomeric sites only as

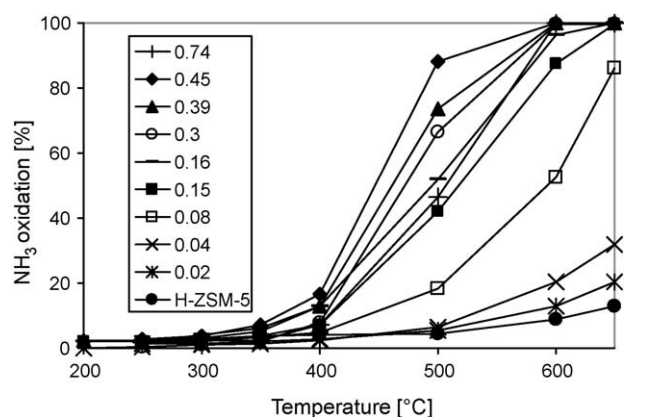


**Fig. 4.**  $\text{NH}_3$  oxidation as a function of temperature over various loading Fe-ZSM-5 catalysts. Main product:  $\text{N}_2$ . Side-product: NO (becomes noticeable above 500 °C). Reaction conditions: 1000 ppm  $\text{NH}_3$ , 10%  $\text{O}_2$ , 5%  $\text{H}_2\text{O}$  and  $\text{N}_2$  balance. GHSV =  $52,000 \text{ h}^{-1}$ .

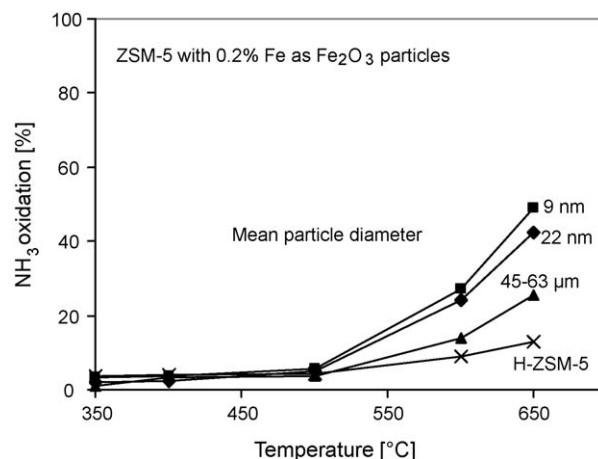


**Fig. 5.**  $\text{NH}_3$  conversion as a function of temperature over H-ZSM-5 samples coated with equal amounts of  $\text{Fe}_2\text{O}_3$  (0.2% Fe), with various particle sizes. Reaction conditions: 1000 ppm  $\text{NH}_3$ , 10%  $\text{O}_2$ , 5%  $\text{H}_2\text{O}$  and  $\text{N}_2$  balance. GHSV =  $52,000 \text{ h}^{-1}$ .

suggested by this study) possess the same TOF value, whereas the nonactive sites have a TOF value near zero.

The kinetic analysis in the appendix demonstrates that a first-order rate law, with respect to NO, is sufficiently accurate to describe the kinetic behavior of the Fe-ZSM-5 samples in our SCR tests in the temperature range of 210–400 °C. Hence, the SCR activities could be quantified by apparent first-order rate constants according to Eq. (6). Fig. 8 shows a reasonable correlation between the reaction rate constants of the catalyst at 250 °C and the concentration of monomeric iron ions. This result further verifies the relevance of this iron species for low temperature activity.

The results in Fig. 7 let us conclude that, at intermediate and high temperatures, clustered species also significantly contribute to the overall SCR activity. The TOF values, calculated with respect to monomeric iron species, were more or less equal up to 300 °C, but diverged at 350 °C and 400 °C, where higher TOF values were found for all samples with  $\text{Fe}/\text{Al} > 0.02$ . Because samples with  $\text{Fe}/\text{Al} > 0.02$  contain increasing fractions of clustered species, this result implies the participation of iron clusters in the SCR reaction above 300 °C. Moreover, it is interesting to note that the TOF values increased from  $\text{Fe}/\text{Al} = 0.02$  or 0.04 up to 0.15 and then decreased again with increasing exchange degree in this temperature region. This behavior could be interpreted such that, between 300 °C and 400 °C, higher clustered species (oligomers), which dominate in samples with  $\text{Fe}/\text{Al} = 0.3, 0.39$  and 0.74, contributed less to the

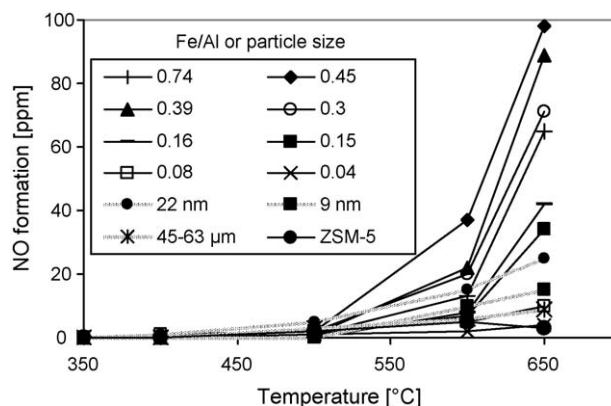


**Fig. 6.** NO formation as a function of temperature over various loading Fe-ZSM-5 catalysts and H-ZSM-5 samples coated with equal amounts of  $\text{Fe}_2\text{O}_3$  (0.2% Fe), with various particle sizes. Reaction conditions: 1000 ppm  $\text{NH}_3$ , 10%  $\text{O}_2$ , 5%  $\text{H}_2\text{O}$  and  $\text{N}_2$  balance. GHSV =  $52,000 \text{ h}^{-1}$ .



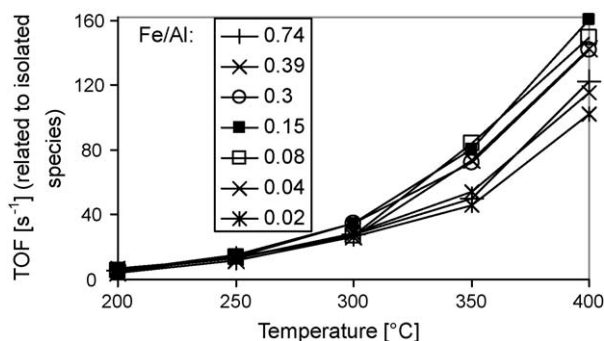


Fig. 7. TOF with respect to monomeric species for Fe-ZSM-5 at  $T = 200^{\circ}\text{C}$ ,  $250^{\circ}\text{C}$ ,  $300^{\circ}\text{C}$ ,  $350^{\circ}\text{C}$  and  $400^{\circ}\text{C}$ .

overall SCR activity than did lower clustered species (e.g., dimers), which were predominantly found in samples with  $\text{Fe}/\text{Al} = 0.04$ ,  $0.08$  and  $0.15$  (Table 1). Because clustering begins with dimers and is followed by oligomers with different nuclearity, dimers should be the second most prevalent species aside from monomeric iron species in the samples with  $\text{Fe}/\text{Al} = 0.04$ ,  $0.08$  and  $0.15$  (Table 1). Consequently, dimers are suspected to be responsible for the rising TOF values at  $T > 300^{\circ}\text{C}$ , while oligomeric species (e.g., trimeric or tetrameric iron species) should generally possess considerably lower TOF values than dimeric and monomeric species between  $300^{\circ}\text{C}$  and  $400^{\circ}\text{C}$ . This assumption agrees with the results shown in Fig. 9, which displays a reasonable correlation between the reaction rate constants of the catalysts at  $350^{\circ}\text{C}$  and the sum of the concentration of monomeric and dimeric iron species.

It should be noted here that in Fig. 9 the sample with  $\text{Fe}/\text{Al} = 0.74$  was assumed to be an outlier, suggesting that this sample contained less dimeric species than was calculated in Table 1; however, the activity pattern of this sample allowed us to draw an additional conclusion that helped us understand the activity of the oligomeric species. Fig. 7 reveals that, between  $200^{\circ}\text{C}$  and  $350^{\circ}\text{C}$ , the TOF values of the sample  $\text{Fe}/\text{Al} = 0.02$  agreed well with the value for  $\text{Fe}/\text{Al} = 0.74$ , whereas at  $400^{\circ}\text{C}$ , the TOF value of the sample  $\text{Fe}/\text{Al} = 0.74$  was about 20% higher. These data indicate that, in the sample  $\text{Fe}/\text{Al} = 0.74$ , species other than monomers became important for SCR at  $400^{\circ}\text{C}$ , which were likely oligomeric iron sites.

The catalytic results can be combined with the estimated concentrations of different species in Table 1 to obtain a rough idea of the TOF values of the monomeric and dimeric iron species as a function of temperature (Table 2). The TOF values of monomeric species between  $200^{\circ}\text{C}$  and  $300^{\circ}\text{C}$  can be easily calculated from samples with  $\text{Fe}/\text{Al} = 0.02$  and  $0.04$ , respectively, as these samples contain almost exclusively monomeric iron ions. On the basis of

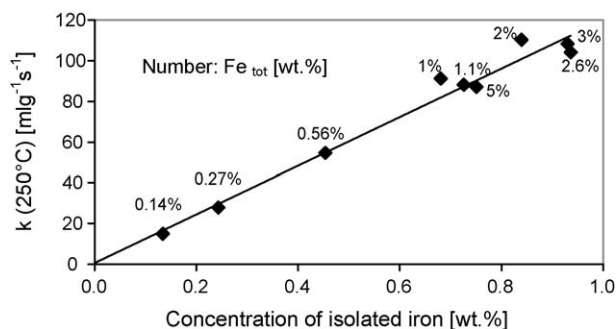


Fig. 8. First-order rate constant for the SCR reaction at  $250^{\circ}\text{C}$  as a function of the calculated concentration of monomeric iron sites.

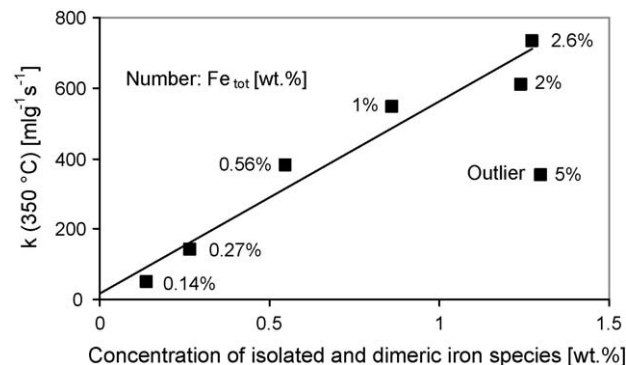


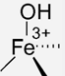
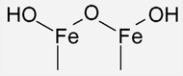
Fig. 9. First-order rate constant for the SCR reaction at  $350^{\circ}\text{C}$  as a function of the sum of the calculated concentrations of monomeric and dimeric iron sites.

the results in Fig. 7, the TOF values for monomeric species were estimated from NO conversions of 2–20% and found to be  $7 \pm 0.5 \text{ s}^{-1}$ ,  $15 \pm 0.5 \text{ s}^{-1}$  and  $28 \pm 2 \text{ s}^{-1}$  at  $200^{\circ}\text{C}$ ,  $250^{\circ}\text{C}$  and  $300^{\circ}\text{C}$ , respectively (Table 2). Note that the given uncertainty corresponds to the standard deviation of the calculated average values. For estimation of the TOF values for higher temperatures, we extrapolated the TOF values from an Arrhenius plot and found them to be  $45 \pm 2 \text{ s}^{-1}$ ,  $74 \pm 4 \text{ s}^{-1}$  and approximately  $153 \pm 8 \text{ s}^{-1}$  at  $350^{\circ}\text{C}$ ,  $400^{\circ}\text{C}$  and  $500^{\circ}\text{C}$ , respectively.

For the estimation of the TOF values for the dimeric species, we had to return to Fig. 9, where we learned that the observed NO conversion up to  $T = 400^{\circ}\text{C}$  was primarily caused by monomeric and dimeric Fe species. This result means that, for samples with  $\text{Fe}/\text{Al} \leq 0.15$  containing only small amounts of higher clustered species, the contribution of oligomers to the overall SCR activity could be ignored. Therefore, the contribution of the dimeric species to the overall NO conversion can be estimated by subtracting the calculated NO conversion of monomeric species from the measured overall NO conversion between  $300^{\circ}\text{C}$  and  $400^{\circ}\text{C}$ . The NO conversion of the monomeric species could thereby be easily calculated by applying the TOF values of this species reported in Table 2. Table 3 shows calculated NO conversions related to monomeric iron sites, the measured overall NO conversion and the difference between these values. The calculated differences correspond to the NO conversion ascribed to dimeric iron sites for samples with  $\text{Fe}/\text{Al} = 0.08$  and  $0.15$ . On the basis of these calculated NO conversions, we calculated the TOF values for the dimeric species to be approximately  $8 \pm 5 \text{ s}^{-1}$ ,  $27 \pm 10 \text{ s}^{-1}$  and  $58 \pm 13 \text{ s}^{-1}$  at  $300^{\circ}\text{C}$ ,  $350^{\circ}\text{C}$  and  $400^{\circ}\text{C}$ , respectively (Table 2). For estimation of the TOF values for  $200^{\circ}\text{C}$ ,  $250^{\circ}\text{C}$  and  $500^{\circ}\text{C}$ , we extrapolated the TOF values from an Arrhenius plot and found them to be  $\leq 1 \text{ s}^{-1}$ ,  $2 \pm 1 \text{ s}^{-1}$  and about  $270 \pm 80 \text{ s}^{-1}$  at  $200^{\circ}\text{C}$ ,  $250^{\circ}\text{C}$  and  $500^{\circ}\text{C}$ , respectively.

From a comparison of the TOF values in Table 2, it becomes apparent that the ratios of the TOF values of monomeric and dimeric species ( $\text{TOF}_{\text{monomeric}}/\text{TOF}_{\text{dimeric}}$ ) are  $\geq 7$ ,  $7$ ,  $3$ ,  $2$ ,  $1.5$  and  $0.5$  at  $200^{\circ}\text{C}$ ,  $250^{\circ}\text{C}$ ,  $300^{\circ}\text{C}$ ,  $350^{\circ}\text{C}$ ,  $400^{\circ}\text{C}$  and  $500^{\circ}\text{C}$ , respectively. This behavior points to considerably different activation energies of the two species. We estimated the apparent activation energy for both species from an Arrhenius plot according to the Arrhenius equation  $k = A \times e^{-E_a/(RT)}$ . For monomeric species, Arrhenius plots between  $200^{\circ}\text{C}$  and  $300^{\circ}\text{C}$  were obtained by calculating NO conversion rates from the data depicted in Fig. 1 via Eq. (6) from NO conversions  $< 70\%$  for samples with  $\text{Fe}/\text{Al} = 0.02$ ,  $0.04$ ,  $0.08$ ,  $0.15$ ,  $0.3$ ,  $0.39$  and  $0.74$  (Fig. 10). For dimeric species, we used data in Table 3 for samples with  $\text{Fe}/\text{Al} = 0.08$  and  $0.15$  to create the Arrhenius plot between  $300^{\circ}\text{C}$  and  $400^{\circ}\text{C}$  (Fig. 11). Linear regressions were performed and yield the corresponding apparent activation energy for monomeric species to be  $36.3 \pm 0.2 \text{ kJ/mol}$

**Table 2**Overview of TOF values of different iron species at different temperatures and apparent activation energies ( $E_a$ ) of monomeric and dimeric species.

Temperature	Monomeric species  $E_a = 36 \pm 0.2 \text{ kJ/mol}$	Dimeric species  $E_a = 77 \pm 16 \text{ kJ/mol}$	Oligomeric species $\text{Fe}_x\text{O}_y(\text{OH})_z \text{ } x \geq 3$	Particles $\text{Fe}_2\text{O}_3$
200 °C	TOF = $7 \pm 0.5 \text{ s}^{-1}$ (200 °C)	TOF $\leq 1 \text{ s}^{-1,a}$ (250 °C)	–	–
250 °C	TOF = $15 \pm 0.5 \text{ s}^{-1}$ (250 °C)	TOF = $2 \pm 1 \text{ s}^{-1,a}$ (250 °C)	–	–
300 °C	TOF = $28 \pm 2 \text{ s}^{-1}$ (300 °C)	TOF = $8 \pm 5 \text{ s}^{-1}$ (300 °C)	–	–
350 °C	TOF = $45 \pm 2 \text{ s}^{-1,b}$ (350 °C)	TOF = $27 \pm 10 \text{ s}^{-1}$ (350 °C)	–	–
400 °C	TOF = $74 \pm 4 \text{ s}^{-1,b}$ (400 °C)	TOF = $58 \pm 13 \text{ s}^{-1}$ (400 °C)	Active	–
>400 °C	TOF = $153 \pm 8 \text{ s}^{-1,b}$ (500 °C)	TOF = $270 \pm 80 \text{ s}^{-1,a}$ (500 °C)	Active	TOF = $27 \text{ s}^{-1}$ (500 °C)

<sup>a</sup> TOF value was extrapolated from an Arrhenius plot of the TOF values at 300 °C, 350 °C and 400 °C (data not shown).<sup>b</sup> TOF value was extrapolated from an Arrhenius plot of the TOF values at 200 °C, 250 °C and 300 °C (data not shown).**Table 3**Calculated NO conversions related to monomeric iron sites, the measured overall NO conversion and the difference between these values. The calculated differences correspond to the NO conversion ascribed to dimeric iron sites for samples with Fe/Al = 0.08 and 0.15. GHSV = 200,000 s<sup>-1</sup>.

Temperature	Calculated NO conversion of monomeric iron sites [%] <sup>a</sup>		Measured overall NO conversion [%]		Calculated NO conversion of dimeric iron sites [%] <sup>b</sup>	
Fe/Al:	0.08	0.15	0.08	0.15	0.08	0.15
250 °C	3.5	4.7	4.7	5.1	1.2	0.4
300 °C	6.0	8.5	8.7	10.7	2.7	2.2
350 °C	10.2	14.3	18.4	24.6	8.2	10.3
400 °C	16.7	23.2	32.9	49.0	16.2	25.8

<sup>a</sup> Calculated with TOF values in Table 2. Note that the NO conversion of the H-ZSM-5 (Fig. 1) was added to the calculated value.<sup>b</sup> Difference between the overall NO conversion (column three) and the calculated NO conversion corresponding to monomeric iron sites (column two).

and for dimeric species to be  $77 \pm 16 \text{ kJ/mol}$  (Table 2). The values for monomeric species were close to data reported in the literature for Fe-ZSM-5 between 200 °C and 280 °C (35 kJ/mol) [39]. Note that for the estimation of the apparent activation energy of monomeric species, samples with Fe/Al = 0.02 and 0.04 were used because these samples contained primarily monomeric iron sites. The samples with Fe/Al > 0.04 showed slightly higher slopes, which could be attributed to the contribution of the dimeric species, resulting in higher activation energies of 45.1 kJ/mol, 53.1 kJ/mol, 49.8 kJ/mol, 46.3 kJ/mol, 48.8 kJ/mol and 51.3 kJ/mol for samples with Fe/Al = 0.08, 0.15, 0.16, 0.3, 0.39 and 0.74, respectively. These were also close to values obtained for Fe-ZSM-5 between 240 °C and 300 °C (54 kJ/mol) [40] and between 200 °C and 400 °C (45 kJ/mol) [41].

The reason for the high apparent activation energy of the dimeric iron species is ambiguous, but may be explained by the results of Heyden et al. [42]. The authors propose that the

adsorption of water might increase the activation barrier for N<sub>2</sub>O decomposition over Fe-ZSM-5 because the loss of water via dehydration is a slow process. Consequently, one could argue that the dimeric iron species forms a stronger bond with water compared to the monomeric iron sites. This hypothesis is in line with kinetic results depicted in Table 4 and shown in Fig. 14d, which reveal that at 350 °C and 400 °C, NO conversion decreases with increasing H<sub>2</sub>O concentration. Conversely, at low temperature, the NO conversion was more or less independent of the H<sub>2</sub>O concentration. The obtained apparent activation energies let us understand the observed TOF values for monomeric and dimeric species. On the basis of the apparent activation energies, we calculated the apparent relative rate constants, which were then normalized (i.e., multiplied by a certain constant factor, Fig. 12). This factor was chosen in order to attain equal rate constants at 420 °C, as suggested by the interpolated TOF values in Table 2.

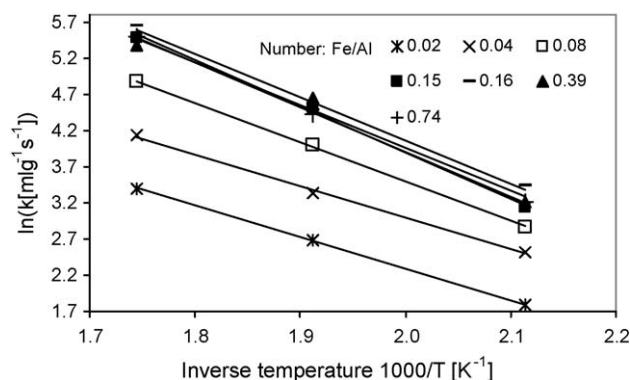


**Fig. 10.** Arrhenius plots of the NO conversion rate constants, calculated from data in Fig. 1 between 200 °C and 300 °C. The apparent activation energies obtained from the regression were 36.3 kJ/mol, 36.2 kJ/mol, 45.1 kJ/mol, 53.1 kJ/mol, 49.8 kJ/mol, 46.3 kJ/mol, 48.8 kJ/mol and 51.3 kJ/mol for samples with Fe/Al = 0.02, 0.04, 0.08, 0.15, 0.16, 0.3, 0.39 and 0.74, respectively.

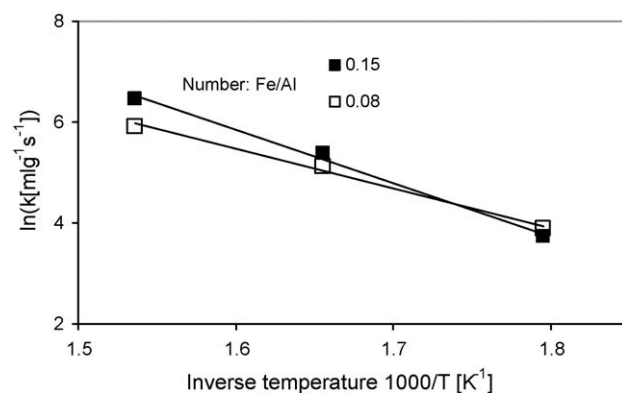


**Fig. 11.** Arrhenius plots of the NO conversion rate constants, calculated from data in Table 3 between 300 °C and 400 °C. The apparent activation energies obtained from the regression were 65 kJ/mol and 88 kJ/mol, respectively, for samples with Fe/Al = 0.08 and 0.15.

**Table 4**

NO conversion at 1000 ppm NH<sub>3</sub>, 1000 ppm NO, 10% O<sub>2</sub> and 5% H<sub>2</sub>O and reaction orders for NO, NH<sub>3</sub>, O<sub>2</sub> and H<sub>2</sub>O in  $-r_{\text{NO}} = k[\text{NO}]^a[\text{NH}_3]^b[\text{O}_2]^c[\text{H}_2\text{O}]^d$ .

Temperature [°C]	NO conversion [%]	a (NO)	b (NH <sub>3</sub> )	c (O <sub>2</sub> )	d (H <sub>2</sub> O)
210 <sup>a</sup>	10.6	0.94	−0.28	0.39	–
250 <sup>a</sup>	21.2	0.90	−0.39	0.39	0.06
300 <sup>a</sup>	48.6	1.00	−0.49	0.39	0.08
325 <sup>a</sup>	71.2	1.02	−0.46	–	–
350 <sup>b</sup>	27.2	1.00	−0.39	0.33	−0.06
400 <sup>b</sup>	53.8	0.93	−0.16	0.16	−0.13

<sup>a</sup> Catalyst Fe-ZSM-5 (0.3); GHSV = 52,000 h<sup>−1</sup>.

<sup>b</sup> Catalyst Fe-ZSM-5 (0.39); GHSV = 200,000 h<sup>−1</sup>.

Fig. 12 illustrates that at low temperature, the overall activity was governed by monomeric iron species, whereas at  $T \approx 350$  °C, the contribution of the dimers became significant to NO conversion.

Our results demonstrate that as the nuclearity of a species is increased, the greater the required temperature to activate this species for catalysis of the SCR reaction. This trend was not only found for monomeric, dimeric and oligomeric species, but also for iron oxide nanoclusters and particles, which were located on the outside of the zeolite pores (Fig. 3). For instance, the 9 nm-sized nanoparticles did not show significant NO conversion up to 350 °C; however, at higher temperatures, the reaction rate started to increase, achieving a TOF value of 27 s<sup>−1</sup> at 500 °C.

In summary, our results allow us to conclude that all iron species are active for NO-SCR with NH<sub>3</sub> and that their contribution to the overall SCR activity strongly depends on temperature. That is, significant conversion begins at higher temperatures with increasing nuclearity of the different species. SCR activity is primarily a result of monomeric species up to temperatures of  $\sim 300$  °C; however, at  $T > 300$  °C, the contribution of the dimeric Fe–O–Fe species become important. In addition, at  $T \geq 400$  °C, the NO conversion due to oligomeric species grow to be considerable and at  $T \geq 450$  °C, Fe<sub>2</sub>O<sub>3</sub> particles even become SCR active.

#### 4.2. Relation between structure of the active site and NH<sub>3</sub> oxidation activity

Analogous to the SCR reaction, the contribution of the different iron sites to NH<sub>3</sub> oxidation activity was investigated. Fig. 4 clearly reveals that the monomeric iron sites displayed no NH<sub>3</sub> oxidation activity up to 500 °C, which contrasts the activity of these species in the SCR reaction; however, oligomeric sites contributed to NH<sub>3</sub> oxidation as early as  $T \geq 350$  °C. The activity

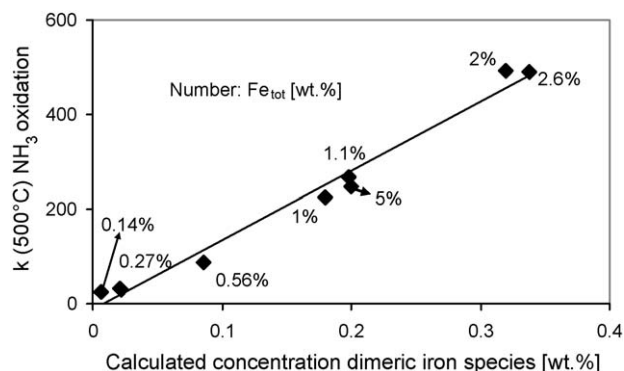


**Fig. 13.** First-order rate constant for NH<sub>3</sub> oxidation as a function of the calculated concentration of clustered iron sites.

pattern in Fig. 4 suggests that NH<sub>3</sub> oxidation was primarily carried out by lower clustered oligomers, or likely dimeric species, because decreasing NH<sub>3</sub> oxidation activities was observed for the sample Fe/Al = 0.74, as compared to sample Fe/Al = 0.45. The importance of dimeric species for NH<sub>3</sub> conversion was confirmed by correlating the catalyst activity (calculated via Eq. (6) from samples with NO conversion <74%) with the calculated amount of dimeric iron species shown in Fig. 13, for which a good relationship was obtained. Analogous to the SCR reaction, it could be speculated that, with rising temperature, the contribution of higher clustered oligomers became significant with rising temperature. This assumption was confirmed by the conversion of NH<sub>3</sub> by Fe<sub>2</sub>O<sub>3</sub> particles of different sizes, which became noticeable at  $T \geq 500$  °C (Fig. 5). The results indicate that the activity for NH<sub>3</sub> conversion decreased with increasing size of the Fe<sub>2</sub>O<sub>3</sub> particles.

The TOF of dimeric species with respect to NH<sub>3</sub> oxidation at 500 °C was calculated from samples with Fe/Al = 0.08, 0.15 and 0.16, as these samples were low in oligomeric species. On the basis of the results depicted in Fig. 4, the TOF values for dimeric species were estimated to be  $70 \pm 13$  s<sup>−1</sup> at 500 °C from NH<sub>3</sub> conversions of between 20% and 50% and the concentrations of dimeric iron species as found in Table 1.

#### 4.3. Explanation for SCR performance as a function of iron content

On the basis of the obtained results, we were able to explain the behavior of the observed SCR rate and its dependence on the exchange degree in Fig. 1a. At  $T \leq 300$  °C, NO<sub>x</sub> conversion is determined by the concentration of monomeric iron sites, which increases with increasing iron content, achieving a maximum and then decreasing again for higher exchange degrees (Fe/Al = 0.74), as inferred from Table 1 by multiplying the iron content by the fraction of monomeric species. For temperatures greater than 500 °C, the NO<sub>x</sub> reduction efficiency is significantly reduced. This observation is due to NH<sub>3</sub> oxidation to N<sub>2</sub> and NO. Because these reactions are favored by clustered species with low nuclearity, likely dimeric species, the decline of the NO conversion is more pronounced with increased iron content but less pronounced for the highly exchanged sample Fe/Al = 0.74. Because of the low NH<sub>3</sub> oxidation activity of the very lowly exchanged samples (Fe/Al = 0.02 and 0.04), they show a deviant behavior with constant (Fe/Al = 0.04) or increasing NO<sub>x</sub> conversions (Fe/Al = 0.02) above 500 °C.

Our results indicate that, for high low temperature activity, an exchange degree of about 0.4 is optimal for ZSM-5 with Si/Al = 14, thereby maximizing the concentration of monomeric iron sites. Additionally, for high activity at  $T > 500$  °C, the exchange degree should not exceed 0.1.

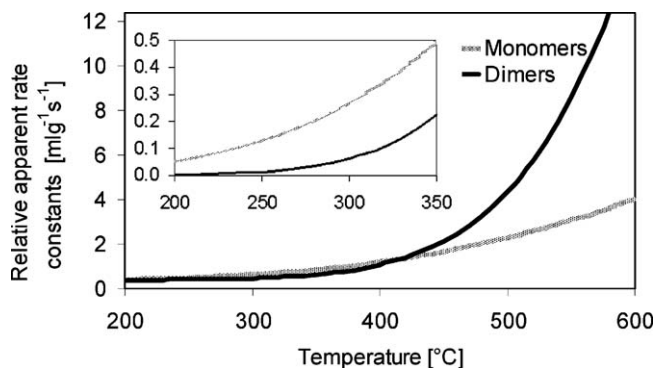


**Fig. 12.** Apparent relative rate constants for monomeric and dimeric iron species as calculated on the basis of the apparent activation energies (Table 2), normalized such that the rate constants at 420 °C were equal (as suggested by TOF values in Table 2).

## 5. Conclusions

The fractions of monomeric, dimeric, clustered and oligomeric species in Fe-ZSM-5, as quantified by calculation [25] were correlated with measured activities in the SCR of NO with NH<sub>3</sub>. This correlation suggests that all iron species are SCR active and that their NO conversion rates show different temperature dependencies. Monomeric species are responsible for SCR activity up to 300 °C, with increasing contributions of dimeric and oligomeric species and even Fe<sub>2</sub>O<sub>3</sub> particles, at higher temperatures. The temperature at which the species substantially contributed to NO conversion was observed to increase with increasing nuclearity of the clusters, which was a function of their activation energies. By comparing the evaluated apparent activation energies for monomeric and dimeric sites, one could understand that, at  $T > 500$  °C, the dimeric species contribution to SCR activity dominates.

With respect to the oxidation of NH<sub>3</sub>, we found that monomeric iron sites, large iron clusters and Fe<sub>2</sub>O<sub>3</sub> particles significantly contribute at temperatures greater than 500 °C. The overall activity below this temperature is governed by small oligomeric, likely dimeric, iron species.

By correlating the calculated concentrations of different iron sites with the catalytic performance of different zeolites, we could understand the catalytic behavior of the different iron species in the SCR reaction, which is a very difficult task on the basis of experimental data alone. Our results contribute to the understanding of the role of the various iron species in the SCR reaction and may have important implications on the preparation of metal-exchanged zeolites. By preparing zeolites with a maximum quantity of single iron sites, good selectivities at high temperatures and high activities at low temperature could be obtained. For Fe-ZSM-5 with a Si/Al ratio of 14, these optimal conditions were best

fulfilled at an exchange degree of about 0.4. On the basis of the presented correlations, we were also able to predict the optimum iron concentrations in other Fe-ZSM-5 SCR catalysts with different Si/Al ratios.

## Appendix A

### A.1. Kinetics

For the correct calculation of the turnover frequencies of the different iron species in Fe-ZSM-5, it was essential to identify the kinetics of the catalyst. In the SCR reaction, the NO conversion rate may depend, in principle, on the concentration of all reactants and reaction products, i.e., NO, NH<sub>3</sub>, O<sub>2</sub> and H<sub>2</sub>O. Accordingly, if no detailed information on the reaction mechanism was used, a simple power-law (Eq. (1)) could be used to model the kinetic data:

$$-r_{\text{NO}} = k[\text{NO}]^a[\text{NH}_3]^b[\text{O}_2]^c[\text{H}_2\text{O}]^d \quad (1)$$

In order to determine the reaction order with respect to  $a$ ,  $b$ ,  $c$  and  $d$  under the applied conditions, we carried out steady-state measurements at a constant temperature for Fe-ZSM-5 (0.3) at GHSV = 52,000 h<sup>-1</sup> and for Fe-ZSM-5 (0.39) at GHSV = 200,000 h<sup>-1</sup>. The measured NO conversions of the catalysts are summarized in Table 4. Please note that for the kinetic measurements, a Fe-ZSM-5 (0.3) sample was used, which was previously exposed to temperatures up to 650 °C, resulting in slight deactivation. Therefore, the activity of the catalyst was slightly lower in comparison to its fresh state, as discernible by comparison of the results in Table 4 with Fig. 1a. For kinetic measurements, the concentration of the different reactants was varied in the range of

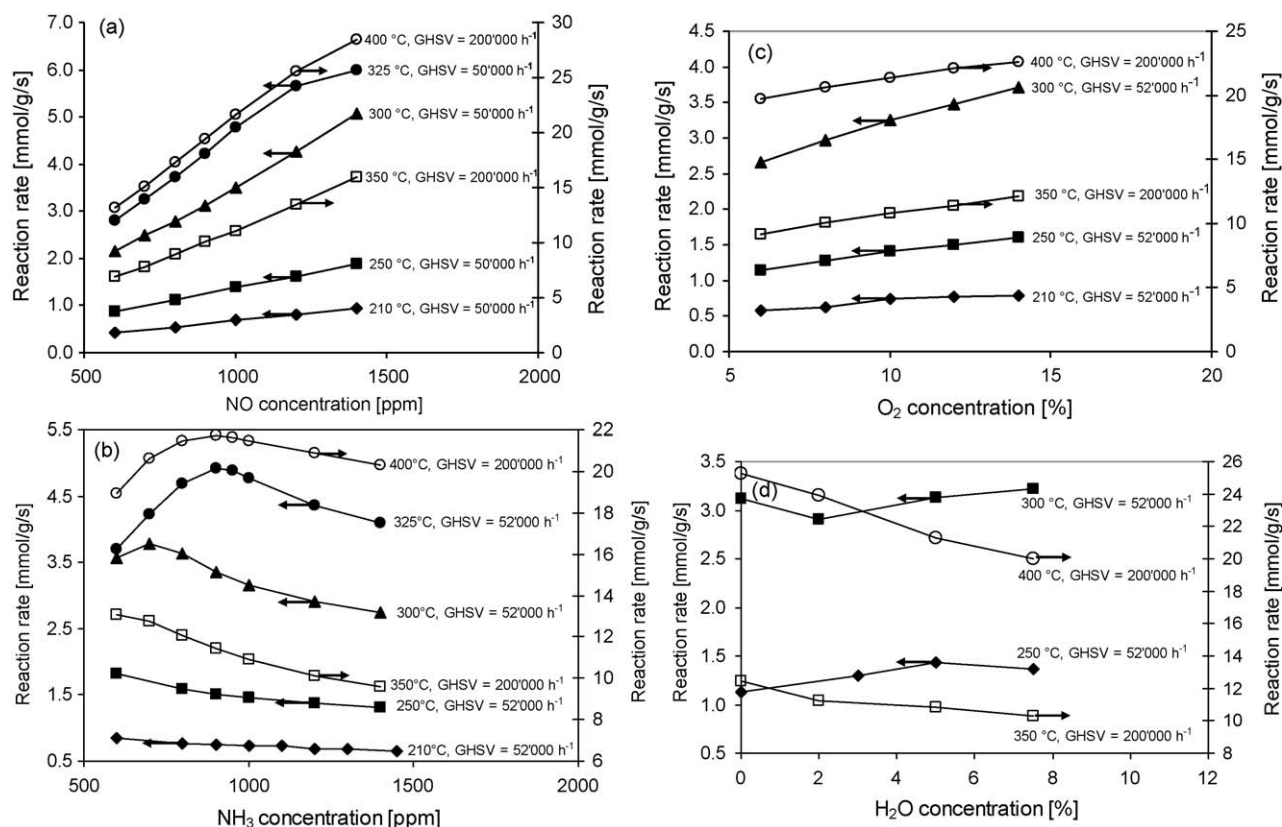


**Fig. 14.** SCR reaction rate as a function of (a) NO, (b) NH<sub>3</sub>, (c) O<sub>2</sub> and (d) H<sub>2</sub>O concentrations. Typical gas composition: 1000 ppm NH<sub>3</sub> and NO, 10% O<sub>2</sub> and 5% H<sub>2</sub>O. GHSV = 52,000 h<sup>-1</sup> (solid symbols) and 200,000 h<sup>-1</sup> (blank symbols).



600–1400 ppm for NO and NH<sub>3</sub> respectively, 6–14% for O<sub>2</sub>, and 0–7.5% for H<sub>2</sub>O. The influence of water on the rate constant was measured at four temperature examples, assuming that the catalysts behaved similarly at the other temperatures.

Fig. 14 shows that NO conversion increases with rising NO and O<sub>2</sub> concentration. The effect of H<sub>2</sub>O concentration and NH<sub>3</sub> on the catalyst was a function of temperature. For H<sub>2</sub>O, at  $T \leq 350$  °C, the NO conversion was observed to be almost independent of the H<sub>2</sub>O concentration, whereas at  $T \geq 350$  °C, the NO conversion slightly increased with decreasing H<sub>2</sub>O concentration. For NH<sub>3</sub>, the NO conversion decreased with rising NH<sub>3</sub> concentration at low temperature, which was in line with an inhibition of the SCR reaction by NH<sub>3</sub> under these conditions [6,43–45]. At intermediate temperatures, the reaction rate first increased, then became virtually independent of NH<sub>3</sub> and finally, decreased with rising NH<sub>3</sub> concentration.

Fig. 15 depicts log plots of the data first presented in Fig. 14. The reaction orders of the reactants were estimated from the slopes in Fig. 15 and the resulting values are given in Table 4. For determining the reaction orders with respect to NH<sub>3</sub>, the slope was taken in the region where the curve showed a linear behavior. Data in Table 4 reveal that the NO conversion rate showed a reaction order of 0.06–(–0.13) for H<sub>2</sub>O, 0.16–0.39 for O<sub>2</sub>, –0.16–(–0.49) for NH<sub>3</sub> and 0.90–1.02 for NO. The measured orders for NO and O<sub>2</sub> are close to the values reported by Huang et al. (0.88–0.94 for NO and 0.36–0.41 for O<sub>2</sub>) [40] and Iwasaki et al. (0.81–0.86 for NO and 0.29–0.34 for O<sub>2</sub>) [39]. The reaction order for NH<sub>3</sub> was slightly lower than the values reported in the literature (–0.15 and –0.11 [40]; –0.11 and –0.21 [39]), while the reaction order for H<sub>2</sub>O could not be compared to the literature data because corresponding studies have not been performed.

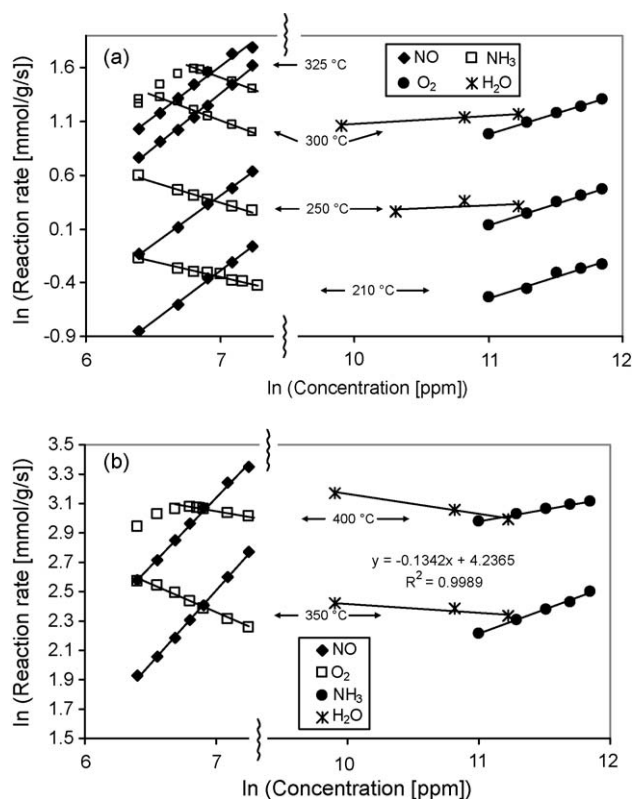


**Fig. 15.** Log-plots of the SCR reaction rate versus NO, NH<sub>3</sub>, O<sub>2</sub> and H<sub>2</sub>O concentrations at (a) GHSV = 52,000 h<sup>–1</sup> for 210 °C, 250 °C, 300 °C and 325 °C and (b) GHSV = 200,000 h<sup>–1</sup> for 350 °C and 400 °C. Data for H<sub>2</sub>O at 210 °C and 325 °C, as well as data for O<sub>2</sub> at 325 °C, were not measured. Typical gas composition: 1000 ppm NH<sub>3</sub> and NO, 10% O<sub>2</sub> and 5% H<sub>2</sub>O.

According to the obtained results, the SCR reaction could be considered to be approximately first-order with respect to NO. O<sub>2</sub> and H<sub>2</sub>O are present in large excess and, therefore, their rate dependencies can be neglected. Consequently, we can rewrite Eq. (1) as:

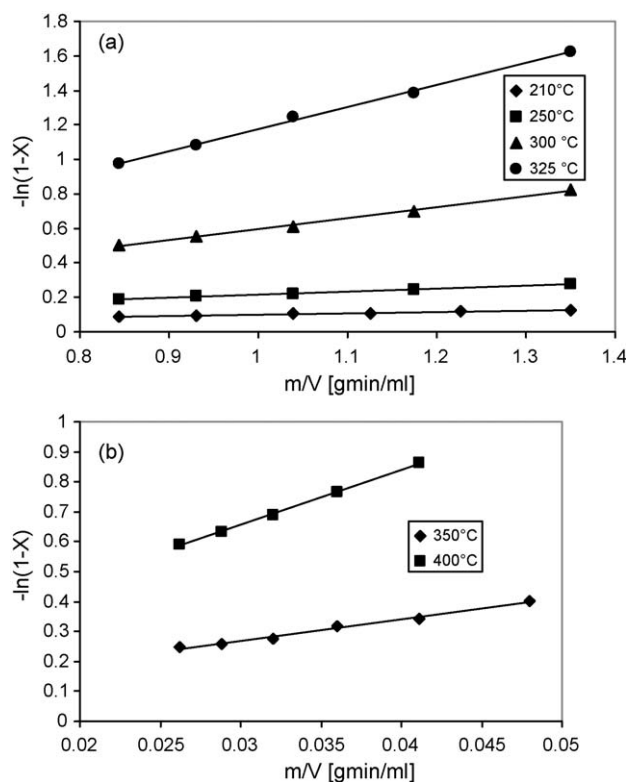
$$-r_{\text{NO}} = k'[\text{NO}][\text{NH}_3]^b \quad (2)$$

Fig. 14 reveals that different reaction regimes have to be considered when describing the dependence of NO conversion on NH<sub>3</sub> concentration. Because it is well known that in the SCR reaction, NH<sub>3</sub> reacts from an adsorbed state, the nonlinear relationship between reaction rate and NH<sub>3</sub> concentration at intermediate temperatures can be attributed to a change in the degree of NH<sub>3</sub> surface coverage ( $\Phi_{\text{NH}_3}$ ) [46]. Therefore, we rewrote Eq. (2) to include a term accounting for the degree of NH<sub>3</sub> surface coverage:

$$-r_{\text{NO}} = k''[\text{NO}]\Phi_{\text{NH}_3} \quad (3)$$

$$\phi_{\text{NH}_3} = \frac{K_{\text{NH}_3} p_{\text{NH}_3}}{1 + K_{\text{NH}_3} p_{\text{NH}_3}} \quad (4)$$

From Eq. (3), it was evident that an increase of the reaction rate with rising NH<sub>3</sub> concentration pointed to an only partly covered catalyst surface. This result agrees with Eq. (4), a decreasing value of  $K_{\text{NH}_3}$  with rising temperature and a decreasing  $p_{\text{NH}_3}$  with a rising NO conversion. With rising  $p_{\text{NH}_3}$ , the coverage increased until complete coverage was achieved. The fact that the rate of NO conversion was nearly zeroth-order with respect to NH<sub>3</sub> at [NH<sub>3</sub>] = 1000 ppm indicated that, at  $T \leq 400$  °C and with a NO conversion of  $\leq 70\%$  and [NO] = [NH<sub>3</sub>] = 1000 ppm, the catalyst surface could be assumed to be almost completely covered with NH<sub>3</sub>. Under these conditions, the reaction rate according to Eq. (4)



**Fig. 16.** First-order plots, with respect to NO, according to Eq. (6) for different feed rates (m/V). (a)  $m = 0.9$  g, GHSV = 40,000–64,000 h<sup>–1</sup> and (b)  $m = 0.12$  g, GHSV = 150,000–275,000 h<sup>–1</sup>.

became almost independent of the  $\text{NH}_3$  concentration and a first-order rate law with respect to NO may be used to describe the kinetic behavior of SCR catalysts:

$$-r_{\text{NO}} = k''[\text{NO}] \quad (5)$$

This simplified the determination of the rate constants  $k''$  from the NO conversion ( $X$ ), because it allowed for the application of the known equation for first-order reactions in a plug flow reactor (under the assumption of the absence of diffusion limitations), which held for low and intermediate temperatures:

$$k'' = \frac{\dot{V}}{m} \times \ln(1 - X) \quad (6)$$

where  $\dot{V}$  is the gas flow rate at the reaction temperature and  $m$  is the catalyst mass [47].

If Eq. (6) is an acceptable approximation,  $-\ln(1 - X)$  should be proportional to  $m/\dot{V}$  at constant temperature and constant NO,  $\text{NH}_3$  and  $\text{O}_2$  concentrations, which was verified in Fig. 16.

## References

- [1] M. Koebel, M. Elsener, M. Kleemann, *Catal. Today* 59 (2000) 335–345.
- [2] J.A. Sullivan, J.A. Doherty, *Appl. Catal. B* 55 (2005) 185–194.
- [3] P. Forzatti, *Catal. Today* 62 (2000) 51–65.
- [4] R.Q. Long, R.T. Yang, *J. Catal.* 188 (1999) 332–339.
- [5] K. Rahkamaa-Tolonen, T. Maunula, M. Lomma, M. Huuhtanen, R.L. Keiski, *Catal. Today* 100 (2005) 217–222.
- [6] O. Kröcher, M. Devadas, M. Elsener, A. Wokaun, N. Soger, M. Pfeifer, Y. Demel, L. Mussmann, *Appl. Catal. B* 66 (2006) 208–216.
- [7] A.Z. Ma, W. Grünert, *Chem. Commun.* (1999) 71–72.
- [8] Q. Sun, Z.X. Gao, H.Y. Chen, W.M.H. Sachtler, *J. Catal.* 201 (2001) 89–99.
- [9] A.A. Battiston, J.H. Bitter, D.C. Koningsberger, *J. Catal.* 218 (2003) 163–177.
- [10] M. Schwidder, M.S. Kumar, A. Brückner, W. Grünert, *Chem. Commun.* (2005) 805–807.
- [11] M.S. Kumar, M. Schwidder, W. Grünert, A. Brückner, *J. Catal.* 227 (2004) 384–397.
- [12] H.Y. Chen, W.M.H. Sachtler, *Catal. Today* 42 (1998) 73–83.
- [13] R.W. Joyner, M. Stockenhuber, *J. Phys. Chem. B* 103 (1999) 5963–5976.
- [14] R.W. Joyner, M. Stockenhuber, *Catal. Lett.* 45 (1997) 15–19.
- [15] F. Heinrich, C. Schmidt, E. Löffler, M. Menzel, W. Grünert, *J. Catal.* 212 (2002) 157–172.
- [16] M. Schwidder, M.S. Kumar, K. Klementiev, M.M. Pohl, A. Brückner, W. Grünert, *J. Catal.* 231 (2005) 314–330.
- [17] R.Q. Long, R.T. Yang, *Catal. Lett.* 74 (2001) 201–205.
- [18] K. Krishna, M. Makkee, *Catal. Today* 114 (2006) 23–30.
- [19] M. Schwidder, W. Grünert, U. Bentrup, A. Brückner, *J. Catal.* 239 (2006) 173–186.
- [20] E.J.M. Hensen, Q. Zhu, R.A. van Santen, *J. Catal.* 220 (2003) 260–264.
- [21] A. Zecchina, M. Rivallan, G. Berlier, C. Lamberti, G. Ricchiardi, *Phys. Chem. Chem. Phys.* 9 (2007) 3483–3499.
- [22] A.A. Battiston, J.H. Bitter, F.M.F. de Groot, A.R. Overweg, O. Stephan, J.A. van Bokhoven, P.J. Kooyman, C. van der Spek, G. Vanko, D.C. Koningsberger, *J. Catal.* 213 (2003) 251–271.
- [23] D. Berthomieu, N. Jardiillier, G. Delahay, B. Coq, A. Goursot, *Catal. Today* 110 (2005) 294–302.
- [24] S. Brandenberger, O. Kröcher, A. Tissler, R. Althoff, *Catal. Rev. Sci. Eng.* 50 (2008) 492–531.
- [25] S. Brandenberger, O. Kröcher, A. Tissler, R. Althoff, *Appl. Catal. A: Genet.* 373 (2010) 168–175.
- [26] M.S. Kumar, On the Nature of Different Fe Sites in Fe-Containing Micro and Mesoporous Materials and Their Catalytic Role in the Abatement of Nitrogen Oxides from Exhaust Gases, Dissertation, Humboldt-Universität, Berlin, 2005.
- [27] G.D. Pirngruber, P.K. Roy, R. Prins, *Phys. Chem. Chem. Phys.* 8 (2006) 3939–3950.
- [28] S. Brandenberger, O. Kröcher, A. Wokaun, A. Tissler, R. Althoff, *J. Catal.* 268 (2009) 297–306.
- [29] D.F. Shantz, C. Fild, H. Koller, R.F. Lobo, *J. Phys. Chem. B* 103 (1999) 10858–10865.
- [30] S. Sklenak, J. Dedecek, C.B. Li, B. Wichterlova, V. Gabova, M. Sierka, J. Sauer, *Angew. Chem. Int. Ed. Engl.* 46 (2007) 7286–7289.
- [31] M.J. Sabater, G. Sastre, *Chem. Mater.* 13 (2001) 4520–4526.
- [32] G. Sastre, V. Fornes, A. Corma, *J. Phys. Chem. B* 106 (2002) 701–708.
- [33] L.M. Jiang, W.L. Sun, J. Kim, *Mater. Chem. Phys.* 101 (2007) 291–296.
- [34] J. Sun, S.B. Zhou, P. Hou, Y. Yang, J. Weng, X.H. Li, M.Y. Li, *J. Biol. Mater. Res. A* 80A (2007) 333–341.
- [35] G. Madia, M. Koebel, M. Elsener, A. Wokaun, *Ind. Eng. Chem. Res.* 41 (2002) 4008–4015.
- [36] P.M. Kleemann, Beschichtung von Cordierit-Wabenkörpern für die selektive katalytische Reduktion von Stickoxiden, Dissertation, Nr. 13401, ETH, Zürich, 1999.
- [37] J. de Graaf, A.J. van Dillen, K.P. de Jong, D.C. Koningsberger, *J. Catal.* 203 (2001) 307–321.
- [38] M. Iwasaki, K. Yamazaki, K. Banno, H. Shinjoh, *J. Catal.* 260 (2008) 205–216.
- [39] M. Iwasaki, K. Yamazaki, H. Shinjoh, *Appl. Catal. A: Genet.* 366 (2009) 84–92.
- [40] H.Y. Huang, R.Q. Long, R.T. Yang, *Appl. Catal. A* 235 (2002) 241–251.
- [41] M. Devadas, O. Kröcher, A. Wokaun, *React. Kinet. Catal. Lett.* 86 (2005) 347–354.
- [42] A. Heyden, B. Peters, A.T. Bell, F.J. Keil, *J. Phys. Chem. B* 109 (2005) 1857–1873.
- [43] H. Sjøvall, L. Olsson, E. Fridell, R.J. Blint, *Appl. Catal. B* 64 (2006) 180–188.
- [44] S.A. Stevenson, J.C. Vartuli, C.F. Brooks, *J. Catal.* 190 (2000) 228–239.
- [45] A. Grossale, I. Nova, E. Tronconi, *Catal. Today* 136 (2008) 18–27.
- [46] M. Koebel, M. Elsener, *Chem. Eng. Sci.* 53 (1998) 657–669.
- [47] O. Levenspiel, *Chemical Reaction Engineering*, John Wiley & Sons, New York, 1999.